Medium Effects in Antibody-Catalyzed Reactions

CRISTINA LEWIS, THOMAS KRÄMER, SUZANNE ROBINSON, DONALD HILVERT*

Catalytic antibody technology has been used to explore the contribution of medium effects to the overall rate of an enzyme-catalyzed reaction. An antibody generated against a derivative of 2-acetamido-1,5-napthalenedisulfonate efficiently catalyzes the decarboxylation of 5-nitro-3-carboxybenzisoxazole. This unimolecular reaction is not susceptible to general acid-base catalysis but is highly sensitive to microenvironment; thus, it provides a simple chemical model for biologically important decarboxylations. The 10^4-fold rate acceleration observed for the antibody reflects the kinetic advantage of the low-dielectric environment of the binding pocket acting to destabilize the substrate by desolvation and to stabilize the charge-delocalized transition state through dispersion interactions. These results are pertinent to an understanding of solvent effects in enzymic reactions in general and suggest approaches for developing antibody catalysts for numerous other reactions that involve large changes in charge distribution as the reaction coordinate is traversed.

THE HIGH CATALYTIC EFFICIENCY OF enzymes can be ascribed in part to the rate accelerations caused by extraction of reactants from aqueous solution into the low-dielectric environment of a protein binding site. In general, however, it is experimentally difficult to measure the extent to which medium effects contribute to the overall rate enhancement of an enzyme-catalyzed reaction because of the additional contributions of proximity effects and individual catalytic groups to the overall complex catalytic mechanism. Catalytic antibody technology (*1*) now makes it possible to examine this mechanistic issue by using a unimolecular model reaction and a tailor-made protein binding pocket.

The decarboxylation of 3-carboxybenzisoxazoles (Fig. 1) is remarkably sensitive to solvent effects and has been widely used to probe the microenvironment of micelles, vesicles, and synthetic polymers (*2*). In aqueous solution, carboxylate **1** has a half-life of several hours at room temperature. However, as the solvent is changed from protic to aprotic, the rate of decomposition can increase by as much as 10^8-fold. Kemp and co-workers have shown that this transformation is a concerted, intermediateless process and have ascribed the dramatic solvent-induced catalysis to two opposing factors: (i) stabilization of the carboxylate in aqueous solution through hydrogen bonding and (ii) stabilization of the extensively charge-delocalized transition state in organic solvents through dispersion interactions (*3*). Because dipolar, aprotic solvents effectively mimic the low-dielectric environment of a protein binding pocket, we reasoned that it should be possible to promote the decarboxylation of **1** in an antibody combining site and evaluate the contribution of solvent effects to catalysis in proteins.

In order to elicit an antibody binding site capable of catalyzing the decarboxylation of 3-carboxybenzisoxazoles, we used the 2-bromoacetamido-1,5-naphthalenedisulfonate derivative **3** as a hapten (*4*). The naphthalene portion of the hapten was expected to elicit a hydrophobic binding pocket of appropriate size. As charge complementarity is a common motif in antibody-antigen complexes, we anticipated that the negatively charged sulfonate groups might induce positively charged residues within the combining site that could provide the binding energy necessary to force the carboxylate anion into a low-dielectric microenvironment. Although hydrogen bonding to the substrate carboxyl group of **1** abolishes the large rate accelerations in organic solvents (*3*), Kemp *et al.* showed in a model study that proximal electrostatic interactions have no influence on the catalytic effects associated with solvent change (*5*).

The keyhole limpet hemocyanin conjugate of **3** is very immunogenic, and immunized 129 GIX$^+$ mice display high serum titers after a single boost. In one fusion we obtained 1200 hybridomas that secreted antibody specific for the hapten (*6*). Tissue culture supernatants were screened directly for decarboxylase activity in sets of 96 with a kinetic microplate reader. The conversion of 5-nitro-3-carboxybenzisoxazole into 2-cyano-4-nitrophenol served as the colorimetric assay reaction (*7*). In this way, we identified a panel of 25 antibodies (2% of total) that have significant activity over the background rate. The corresponding hybridomas were subcloned, propagated in mouse ascites, and purified (*8*).

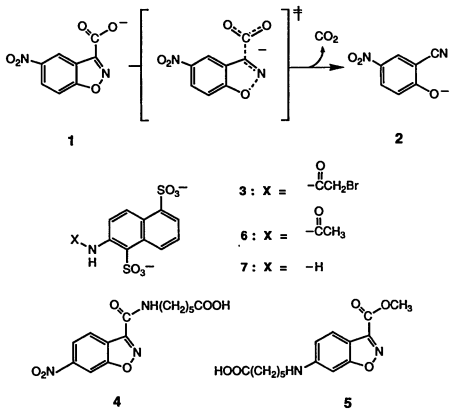

Fig. 1. Conversion of 5-nitro-3-carboxybenzisoxazole **1** to 2-cyano-4-nitrophenol **2**; structures of the haptens **3**, **4**, and **5**, inhibitor **6**, and fluorophore **7**.

In preliminary assays, the antibody isolated from the hybridoma cell line 21D8 possessed considerable decarboxylase activity and was characterized in detail (*9*). Several control experiments confirmed that the observed catalysis is associated with the induced immunoglobulin binding site: (i) the rate of the reaction is linearly proportional to antibody concentration; (ii) nonspecific immunoglobulins and heat-denatured 21D8 have no catalytic activity; and (iii) the haptenic 2-acetamido-1,5-naphthalenedisulfonate **6** is a potent competitive inhibitor, binding to 1.1 ± 0.1 sites per antibody combining site with an inhibition constant K_i = 6.4 ± 0.5 nM [Fig. 2; (*10*)].

Saturation kinetics were observed at high substrate concentrations, consistent with a simple kinetic scheme in which substrate and antibody combine to form a Michaelis-type complex prior to the carbon-carbon bond-breaking step:

$$E + S \underset{k_{-1}}{\overset{k_1}{\rightleftharpoons}} ES \xrightarrow{k_{cat}} \text{products}$$

where k_1, k_{-1}, and k_{cat} are rate constants and E, S, and ES refer to the respective concentrations of the antibody and of free and bound substrate. We obtained the steady-state kinetic parameters k_{cat} = 17 ± 1 min^{-1} and K_m = 168 ± 20 μM at 20°C in 10 mM tris-HCl (pH 8.0) for 5-nitro-3-carboxybenzisoxazole. The antibody-catalyzed rate is pH-independent between pH 5 and 9, and there is no solvent isotope effect on k_{cat} (*11*). The reaction product, 2-cyano-4-nitrophenol, is a competitive inhibitor of catalysis with a K_i value of 21 μM (Fig. 3). Increasing concentrations of sodium chloride inhibit the reaction, presumably because chloride competes for an anion binding site within the induced pocket.

Comparison of the first-order rate constant for conversion of bound starting material into bound product (k_{cat}) with the first-order rate constant for the uncatalyzed decarboxylation in aqueous buffer (k_{un}) provides a direct measure of the chemical effi-

Departments of Chemistry and Molecular Biology, Research Institute of Scripps Clinic, 10666 North Torrey Pines Road, La Jolla, CA 92037.

*To whom correspondence should be addressed.

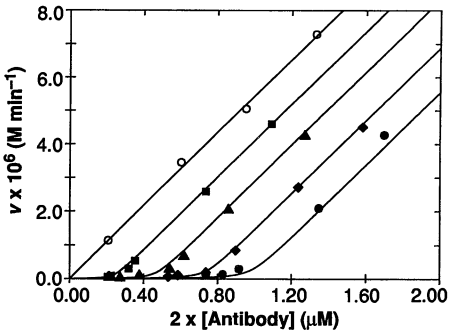

Fig. 2. Dependence of reaction velocity on antibody concentration measured in the presence of 120 μM substrate and different concentrations of tight-binding inhibitor **6**: 0 (○); 0.20 (■); 0.38 (▲); 0.60 (◆); and 0.80 μM (●). Data were fit to Eqs. 1 or 2 (*10*) and plotted with the Minsq nonlinear least-squares curve-fitting program.

ciency of the antibody catalyst. Under the assay conditions given above, we found that k_{cat}/k_{un} = 19,000. In terms of catalytic efficiency, the catalytic antibody is thus superior to a variety of microheterogeneous systems known to catalyze the decarboxylation of carboxybenzisoxazoles, including cationic micelles, crown ethers, and polymeric quaternary ammonium salts (*2, 12*). More importantly, detailed characterization of the chemically well-defined antigen-combining site of 21D8 provides a way to compare directly the reactivity observed in organic model systems to that observed in protein catalysis.

The decomposition of **1** is known to be insensitive to general acid-base catalysis and stereochemical constraints, suggesting that the large rate acceleration provided by the catalytic antibody can be ascribed entirely to medium effects. In order to probe the active site environment of 21D8, the fluorescent hapten analog 2-aminonaphthalene-1,5-disulfonate **7** was chosen as a reporter group; like **6**, this fluorophore is a tight-binding competitive inhibitor of the antibody, displaying 1.3 ± 0.3 binding sites per immunoglobulin combining site with a K_i of 23.1 ± 0.6 nM (*10*). The fluorescence spectrum of **7** bound to excess 21D8 displays a 20-nm blue shift in emission λ_{max}, which is consistent with movement of the probe from an aqueous milieu into an apolar environment (*13*). The accessibility of the antibody binding pocket to solvent was assessed by measuring the ability of small molecules to quench the fluorescence of the bound fluorophore (*14*). Although acrylamide efficiently quenches the fluorescence of the free fluorophore, it has no significant effect on the fluorescence of bound **7** (Fig. 4). Similar results were observed if iodide rather than acrylamide was used as the quencher. Thus, the antibody combining site affords nearly complete protection of the bound fluorophore from small solvent-associated molecules.

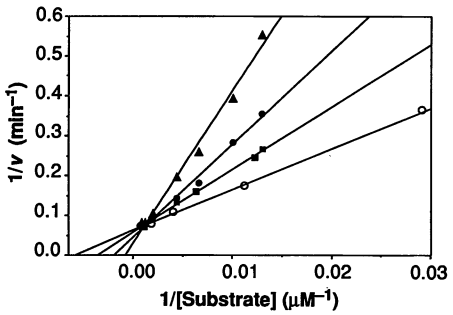

Fig. 3. Lineweaver-Burk plot showing competitive inhibition by product. Assays were performed in the presence of 0 (○), 5 (■), 25 (●), and 50 μM 2-cyano-4-nitrophenol (▲). The K_i was determined from a linear replot of $K_{m_{app}}$ versus inhibitor concentration.

The extent of desolvation by the antibody was determined more directly by measuring the accessibility of water molecules to an environmentally sensitive fluorophore within the binding pocket. Because the fluorescent probe 1,8-anilinonaphthalenesulfonate (1,8-ANS) is also a tight-binding competitive inhibitor of 21D8 [K_i = 328 ± 21 nM, 0.95 ± 0.03 binding sites per Fab; (*15*)], we exploited its environmental sensitivity to probe the antibody active site. The quantum yield Q of 1,8-ANS is dramatically enhanced upon transfer from an aqueous to an apolar environment (Q = 0.004 in an aqueous solution compared with 0.68 in dioxane). Furthermore, free 1,8-ANS is 2.5 times more fluorescent in D_2O than in H_2O (*16*). Thus, measurement of the ability of D_2O to enhance the fluorescence of the bound fluorophore provides a direct estimate of the accessibility of water molecules to the binding pocket. Upon binding to excess 21D8, 1,8-ANS displayed a dramatic increase in fluorescence intensity (Q = 0.99) accompanied by a 58-nm blue shift in emission λ_{max} (*17*). Such an enhancement of fluorescence is similar to that observed when 1,8-ANS is bound to the highly apolar heme binding site of apomyoglobin (*18*). We confirmed that free 1,8-ANS displays a solvent deuterium-isotope effect of 2.5 (Q_D/Q_H in 99% D_2O = 2.49); however, the fluorophore bound to excess 21D8 displays no significant deuterium-isotope effect (Q_D/Q_H = 1.01). Clearly, the binding site for 1,8-ANS is apolar and is nearly completely inaccessible to water molecules when occupied. The sum of the fluorescence and kinetic inhibition data for these two naphthalene-derived fluorophores suggests that 21D8 can potentially effect catalysis by performing two tasks: first, destabilization of a substrate by stripping the carboxylate of its hydration shell and thereby protecting it from hydrogen-bonding interactions with solvent; and second, stabilization of the charge-delocalized transition state by promoting dispersion interactions within the hydrophobic microenvironment. In essence, the immunoglobulin binding site provides an organized medium of low dielectric strength in which to carry out the reaction.

The thermodynamic origin of the antibody's rate acceleration is intriguing. Kemp and co-workers noted, and we have confirmed (Table 1), that the dramatic solvent-assisted rate acceleration seen for the decarboxylation of 3-carboxybenzisoxazoles is due entirely to a lowering of the enthalpy of activation $\Delta H^{\ddagger}$ (*3*). The entropy of activation $\Delta S^{\ddagger}$ is very favorable in aqueous buffer [16 entropy units (e.u.) for the 5-nitro derivative] and does not change appreciably for the reactions carried out in dipolar aprotic solvents such as acetonitrile. This highly favorable $\Delta S^{\ddagger}$ presumably reflects the liberation of ordered solvent molecules from the substrate. For 21D8, the observed rate acceleration over that obtained in aqueous solution is also due to a more favorable $\Delta H^{\ddagger}$ (Table 1). However, the antibody-catalyzed decarboxylation is mechanistically distinct from the solvent-accelerated process in that its $\Delta S^{\ddagger}$ is considerably less favorable. Similar thermodynamic parameters have been reported for polymers and cationic micelles that catalyze carboxybenzisoxazole decarboxylation (*12*). One plausible explanation

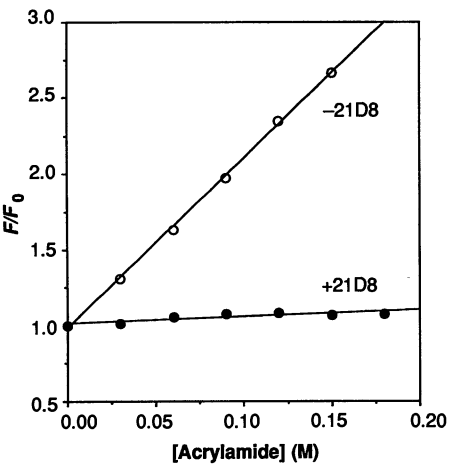

Fig. 4. Stern-Volmer plot of fluorescence quenching of **7** by acrylamide. Fluorescence was measured in the presence or absence of 5.9 μM antibody in 10 mM tris-HCl (pH 8.0), 2 μM **7** and increasing concentrations of acrylamide. Data were analyzed according to the Stern-Volmer equation, $F_0/F = (1 + K_{SV}[Q])e^{V[Q]}$, where F is the fluorescence intensity at a given concentration of quencher Q, F_0 is the fluorescence intensity in the absence of quencher, K_{SV} is the Stern-Volmer constant, and V represents the static quenching constant. In the absence of 21D8, K_{SV} = 9.9 M^{-1} and V = 0.5; in the presence of 21D8, K_{SV} = 0.53 M^{-1} and V = 0.

Table 1. Activation parameters for the decarboxylation reaction of 5-nitro-3-carboxybenzisoxazole. Activation parameters were obtained from linear Arrhenius plots of the temperature dependence data over the range of 10° to 50°C (water and acetonitrile) or 10° to 37°C (21D8). The $\Delta H^{\ddagger}$ values have estimated errors of 0.5 kcal/mol; the $\Delta S^{\ddagger}$ values, 2 e.u.

Solvent (catalyst)	$\Delta H^{\ddagger}$ (kcal/mol)	$\Delta S^{\ddagger}$ (e.u.)
Water	28	16
Acetonitrile	20	14
21D8	19	3

for this observation is that, unlike solvent, the rigid protein matrix that resolvates the substrate upon binding is unable to relax as the reaction approaches the transition state.

The partitioning of a reaction into a less polar medium is an important catalytic mechanism in a number of biologically relevant decarboxylations. For example, this factor is believed to contribute to the observed rate enhancement afforded by histidine decarboxylase, arginine decarboxylase, and by a number of thiamine pyrophosphate-dependent enzymatic reactions (*19*). Indeed, the recently solved crystal structure of histidine decarboxylase from *Lactobacillus* 30a indicates that the carboxylate binding pocket is predominantly hydrophobic (*20*). As noted by Jencks (*21*), the potential rate accelerations that can be attained by medium effects are enormous. The challenge for the chemist interested in exploiting this mechanism in catalyst design is not only to engineer an apolar binding site, but also to generate sufficient binding energy necessary to force the substrate into the destabilizing environment. In this respect, we note that haptens **4** and **5** failed to induce antibodies that could catalyze carboxybenzisoxazole decarboxylations. These particular experiments may have failed because the available binding energy was insufficient to pay for the cost of burying the substrate carboxylate in a hydrophobic pocket, or because these haptens elicited hydrogen-bonding interactions that inhibited catalysis.

Our characterization of a simple unimolecular reaction as a model system suggests that desolvation by a specifically tailored protein binding site can contribute at least four orders of magnitude toward the rate enhancement. Even larger effects may ultimately be accessible by engineering the number and placement of complementary charges within the low-dielectric environment of the active site. The potential for medium effects to contribute to the overall rate acceleration merits extending this strategy to the development of antibody catalysts of increasing sophistication and practical utility. Reactions that display a large change in charge localization, including decarboxylations, aldol condensations bimolecular nucleophilic substitutions (*22*), and phosphate ester hydrolyses (*23*), would be expected to be particularly amenable to such design strategies.

REFERENCES AND NOTES

1. For reviews, see P. G. Schultz, R. A. Lerner, S. J. Benkovic, *Chem. Eng. News* **68**, 26 (1990); D. Hilvert, in *Biomimetic Polymers*, C. G. Gebelein, Ed. (Plenum, New York, 1990), pp. 95–113.
2. S. C. Shah and J. Smid, *J. Am. Chem. Soc.* **100**, 1426 (1978); C. A. Bunton *et al.*, *ibid.* **95**, 3262 (1973); F. P. Schmidtchen, *J. Chem. Soc. Perkin Trans. II* **1986**, 135 (1986).
3. D. S. Kemp, D. D. Cox, K. G. Paul, *J. Am. Chem. Soc.* **97**, 7312 (1975); D. S. Kemp and K. G. Paul, *ibid.*, p. 7305; M. L. Casey, D. S. Kemp, K. G. Paul, D. D. Cox, *J. Org. Chem.* **38**, 2294 (1973).
4. Substrate **1** and product **2** were synthesized as described (*3*). Hapten **3** was synthesized from 2-aminonaphthalene-1,5-disulfonate and bromoacetyl chloride under Schotten-Baumann conditions. The carrier proteins (bovine serum albumin or keyhole limpet hemocyanin) were modified with 2-iminothiolane (Traut's reagent) at pH 8.0 to convert surface amine residues to thiols. The modified proteins were purified by gel filtration prior to conjugation with **3** in 0.1 M sodium phosphate (pH 7.5), 0.1 M NaCl. Epitope density ranged from 11 to 20 haptens per protein molecule. Hapten **4** was prepared by reaction of 6-nitro-1,2-benzisoxazole-3-carboxyhydrazide [S. S. Berg and E. W. Parnell, *J. Chem. Soc.* **1961**, 5275 (1961)] with isoamyl nitrite in a mixture of dry dimethylformamide and 4 M HCl in dioxane, followed by the addition of 6-aminohexanoic acid. The product was purified by extraction and silica gel chromatography before reaction with *N,N'*-disuccinimidyl carbonate to form the activated ester, which was in turn purified by silica gel chromatography prior to coupling to unmodified carrier protein. Hapten **5** was synthesized by reaction of glutaric anhydride with 6-amino-3-carbomethoxybenzisoxazole (*3*); the activated ester was then prepared by reaction with *N,N'*-disuccinimidyl carbonate and purified by silica gel chromatography before coupling to unmodified carrier protein. Inhibitor **6** was prepared by Zn reduction of **3** followed by recrystallization. All of the synthesized compounds showed satisfactory spectroscopic data.
5. D. S. Kemp, J. Reczek, F. Vellaccio, *Tetrahedron Lett.* **8**, 741 (1978).
6. Standard protocols were used to generate and characterize hybridomas produced by fusion of mouse spleen cells with SP2/0+ myeloma cells [E. Harlow and D. Lane, *Antibodies: A Laboratory Manual* (Cold Spring Harbor Laboratory, Cold Spring Harbor, NY, 1988)].
7. In a total volume of 100 μl, 80 μl of tissue culture supernatant fluid was incubated in the presence of 400 μM substrate in 2 mM Hepes (pH 8). Product formation was monitored at 380 nm for 1 hour; assays performed with substrate alone or with substrate and 40% dimethyl sulfoxide served as the negative and positive controls, respectively.
8. Subcloning, propagation in (BALB/c × 129 GIX^{+})F_1 mouse ascites, and purification by ammonium sulfate precipitation and DEAE ion-exchange chromatography were performed as previously described [D. Hilvert, S. H. Carpenter, K. D. Nared, M-T. M. Auditor, *Proc. Natl. Acad. Sci. U.S.A.* **85**, 4953 (1988)]. Monoclonal antibodies were further purified by FPLC (fast protein liquid chromatography) affinity chromatography on protein G Sepharose, followed by FPLC ion-exchange chromatography (MonoQ HR 10/10).
9. Reaction velocities measured in the presence of 10 mM tris-HCl (pH 8.0) were determined spectrophotometrically by measuring the initial linear rate of product formation at 380 nm using the experimentally determined extinction coefficient ε_{380} = 10,600 M^{-1} cm^{-1}. The rate constant for the spontaneous decarboxylation of 5-nitro-3-carboxybenzisoxazole was determined under specific assay conditions and was in agreement with literature values (*3*).
10. *Kinetic data were fit to the following equation for* tight-binding inhibition:

$$\log v = \log \{(M/2)\,[AE - I - K_i + [(K_i + AE - I)^2 + 4\,K_i\,I]^{1/2}\} \quad (1)$$

or, for graphical presentation of the data:

$$v = \{(M/2)\,[AE - I - K_i + [(K_i + AE - I)^2 + 4K_i\,I]^{1/2}]\} \quad (2)$$

where v is the reaction velocity, E is the concentration of enzyme, M is the maximum velocity in the absence of inhibitor, A is the number of active sites, and K_i is the apparent inhibition constant at a particular substrate concentration. The course of the reaction proceeded linearly and at a similar rate whether the reaction was initiated with antibody or with substrate after preincubation of antibody and inhibitor, indicating that the inhibition by **6** is reversible. Competitive inhibition was demonstrated by a linear replot of apparent K_i versus substrate concentration [J. W. Williams and J. F. Morrison, *Methods Enzymol.* **63**, 437 (1979); C. E. Grimshaw *et al.*, *Biochemistry* **28**, 5343 (1989)]. Error limits of ±1 SD are used throughout this report.
11. The dependence of velocity on pH was determined as described (*9*), except the buffer contained 5 mM each of citric acid, imidazole, tris-HCl, and piperazine adjusted to the appropriate pH. Reaction velocities were corrected for minor pH-dependent changes in the rate of spontaneous decarboxylation and in ε_{380} of the product. The solvent deuterium isotope effect was determined in 10 mM tris-HCl (pD 8.4) in the presence of 97% D_2O.
12. J. Suh *et al.*, *J. Am. Chem. Soc.* **98**, 7060 (1976); C. A. Bunton *et al.*, *J. Org. Chem.* **40**, 1321 (1975); T. Kunitake *et al.*, *J. Am. Chem. Soc.* **102**, 7877 (1980); J. Smid *et al.*, *ibid.* **97**, 5932 (1975).
13. Fluorescence measurements were made on a Shimadzu RF 5000U spectrofluorimeter equipped with a FDU-3 data processor: excitation, 350 nm; emission, 360 to 600 nm. Unless otherwise indicated, all measurements were made in 10 mM tris-HCl (pH 8.0).
14. M. R. Eftink and C. A. Ghiron, *Anal. Biochem.* **114**, 199 (1981).
15. Bis-free 1,8-ANS was obtained from Molecular Probes. Inhibition of 21D8 by the fluorophore was characterized as described in Fig. 3. Fluorescence spectra excitation, 372 nm; emission, 400 to 600 nm. Binding of 1,8-ANS to the antibody was measured fluorometrically by using the method of Klotz *et al.* [I. M. Klotz, F. M. Walker, R. B. Pivan, *J. Am. Chem. Soc.* **68**, 1486 (1946)] which assumes that all binding sites are identical and noncooperative. Increasing concentrations of fluorophore (43 to 700 nM) were added to different fixed concentrations of antibody (100 nM to 16 μM) and the fluorescence was monitored at emission λ_{max} = 455 nm. In the presence of excess antibody, the fluorescence intensity was linearly dependent on the concentration of 1,8-ANS in the range indicated. The K_d determined by this method (136 ± 8 nM) was in reasonable agreement with the experimentally determined K_i.
16. L. Stryer, *Science* **162**, 526 (1968); D. C. Turner and L. Brand, *Biochemistry* **7**, 3381 (1968).
17. Quantum yields were measured by spectral integration with subtraction of appropriate blanks (excitation, 372 nm, and emission, 400 to 600 nm) by using as a standard the quantum yield of 1,8-ANS in ethanol [H. H. Seliger, *Methods Enzymol.* **57**, 560 (1978); A. Azzi, *ibid.* **32**, 234 (1974)].
18. L. Stryer, *J. Mol. Biol.* **13**, 482 (1965).
19. J. Crosby, R. Stone, G. E. Lienhard, *J. Am. Chem. Soc.* **92**, 2891 (1970); M. H. O'Leary and G. J. Piazza, *Biochemistry* **20**, 2743 (1981); T. A. Alston and R. H. Abeles, *ibid.* **26**, 4082 (1987).
20. T. Gallagher, E. E. Snell, M. L. Hackert, *J. Biol. Chem.* **264**, 12737 (1989).
21. W. P. Jencks, *Catalysis in Chemistry and Enzymology* (Dover, New York, 1969), pp. 645–650.

22. A. J. Parker, *Chem. Rev.* **69**, 1 (1969).
23. K. W. Y. Abell and A. J. Kirby, *Tetrahedron Lett.* **27**, 1085 (1986).
24. Supported in part by Faculty Research Award FRA369 from the American Cancer Society and by grant GM38273 from the National Institutes of Health (to D.H.), a fellowship from the Jane Coffin Childs Memorial Fund for Medical Research (to C.L.), and a fellowship from the Verband der Chemischen Industrie (to T.K.). We gratefully acknowledge the assistance of S. Miller for preliminary experiments, J. Patel for constructive suggestions, and C. Grimshaw and D. Goodin for helpful discussions about the kinetic analyses of tight-binding inhibitors.

16 April 1991; accepted 19 June 1991

Differential Phosphorylation of the Transcription Factor Oct1 During the Cell Cycle

SUSAN BOSEMAN ROBERTS, NEIL SEGIL, NATHANIEL HEINTZ

Orderly progression through the somatic cell division cycle is accompanied by phase-specific transcription of a variety of different genes. During S phase, transcription of mammalian histone H2B genes requires a specific promoter element and its cognate transcription factor Oct1 (OTF1). A possible mechanism for regulating histone H2B transcription during the cell cycle is direct modulation of Oct1 activity by phase-specific posttranslational modifications. Analysis of Oct1 during progression through the cell cycle revealed a complex temporal program of phosphorylation. A $p34^{cdc2}$-related protein kinase that is active during mitosis may be responsible for one mitotic phosphorylation of Oct1. However, the temporally controlled appearance of Oct1 phosphopeptides suggests the involvement of multiple kinases and phosphatases. These results support the idea that cell cycle–regulated transcription factors may be direct substrates for phase-specific regulatory enzymes.

CYCLING EUKARYOTIC CELLS ALTERnate between mitosis (M phase) and DNA replication (S phase) through an orderly progression of biochemical processes. An example of the maintenance and control of this order is the close coupling of histone gene transcription and the onset of chromosomal DNA synthesis (*1*). In mammalian cells, coordinate induction of the five families of histone genes during S phase is not a result of activation of a single transcription factor, but is achieved through distinct factors that interact with subtype-specific promoter elements (*2–5*). This suggests the existence of a pleiotropic mechanism for regulating the activity of transacting factors with specific functions in S phase of the cell cycle (*4*). A single mechanism with diverse molecular targets might be fundamental to the control of S phase, perhaps regulating factors involved in processes as diverse as transcription and DNA replication.

The transcription factor Oct1 (OTF1) has been implicated in transcriptional activation of a variety of genes (*5, 6*) including the genes encoding histone H2b (*5, 7*). Oct1 stimulates H2b transcription in vitro through its interaction with a sequence that contains the octamer motif (ATTTGCAT), which is evolutionarily conserved in histone H2b genes at a precise position adjacent to the TATA box (*8*). S phase–specific activation of histone H2b genes in vivo and in vitro requires this subtype-specific promoter element (*4, 5*). Oct1 can also stimulate initiation of adenovirus DNA replication in vitro (*9*), raising the possibility that Oct1 may also be involved in chromosomal DNA synthesis. These studies suggest that the activity of Oct1 or an associated protein is modulated in a cell cycle–dependent manner and implicate Oct1 as a target of a general cell cycle regulatory mechanism.

Phosphorylation and dephosphorylation are known to alter nuclear protein activities and interactions at specific phases of cell cycle. For example, both the G2 to M and G1 to S cell cycle transitions are dependent on the activity of cdc2 protein kinase (*10*), which is regulated by specific phosphorylations and dephosphorylations (*11*). Furthermore, phosphorylation of Oct1 in vivo has been demonstrated by transfection of Oct1 constructs into HeLa cells (*12*). We analyzed the phosphorylation state of Oct1 in actively cycling mammalian cells to determine whether differential phosphorylation of Oct1 is correlated with its ability to activate transcription of the H2B gene during the cell cycle.

Polyclonal antiserum to Oct1 (anti-Oct1) (*13*) was used to analyze Oct1 from whole cell extracts prepared from synchronously growing HeLa cells. There was no change in the abundance (Fig. 1B) or rate of synthesis (Fig. 1C) of Oct1 during the cell cycle except in cells arrested in mitosis (Fig. 1C, lane N), where synthesis of Oct1 as well as lamin B (control) was depressed. Synchronized cells were labeled for one hour (pulse-labeled) with [^{32}P]orthophosphate; immunoprecipitation with anti-Oct1 of whole cell extracts produced a pattern of protein bands that migrated in the position expected for Oct1, but that was more complex than the pattern seen by immunoblot analysis (Fig. 1B) or from immunoprecipitates of [^{35}S]methionine-labeled Oct1 (Fig. 1C). The most obvious difference in the Oct1 pattern was from cells blocked in mitosis by nocodazole (N) where there was a dramatic increase in ^{32}P incorporation and a retarded migration. The retarded migration of Oct1 from cells blocked in mitosis was also apparent in the immunoblot (Fig. 1B, lane N) and the [^{35}S]methionine-labeled sample (Fig. 1C, lane N*). In addition to the difference in M phase, there was a difference in the pattern of ^{32}P-labeled Oct1 bands from cells in S phase (+4 and +8 hours) compared to the pattern from cells in G1 and G2+M (G1, +12, +16, +20 hours) or cells blocked at the G1 to S boundary by aphidicolin (A). The middle band was absent in S phase (+4 and +8). The fluorescence-activated cell sorting (FACS) analysis (Fig. 1A) and the pattern of [^{32}P]orthophosphate incorporation into lamin B (Fig. 1D) (*14*) establish that the method used for analysis of the synchronized whole cell extracts is reliable and stage-specific.

The change in Oct1 at mitosis was detected by one-dimensional gel electrophoresis because of the massive increase in ^{32}P-incorporation in nocodazole-blocked cells (N), but variability of the method for resolving differences in Oct1 during interphase prompted the use of two-dimensional gel fractionations. Two-dimensional gel analysis of Oct1 chromatographically purified from logarithmically growing cells (Fig. 2A) indicated that Oct1 can be resolved on the basis of charge into five species and that the different forms of Oct1 are detected by anti-Oct1. Immunoprecipitates of ^{32}P-labeled Oct1 from synchronized cells were also fractionated by two-dimensional gel electrophoresis (Fig. 2B). G1 phase cells (Fig. 2B, panel G1) contained five species of Oct1 that were very similar to the pattern of purified protein (Fig. 2A). The relative labeling of the Oct1 species changed in cells arrested at the G1 to S boundary by aphidicolin (Fig. 2B, panel G1a). The ^{32}P-labeled Oct1 species immunoprecipitated from S phase cells (panel S) differed in relative labeling and migration from those in G1. The labeled Oct1 species from S phase were shifted toward the basic end of the isoelec-

Howard Hughes Medical Institute, Laboratory of Molecular Biology, Rockefeller University, 1230 York Avenue, New York, NY 10021.